Journal of Materials Chemistry

Dynamic Article Links

Cite this: J. Mater. Chem., 2011, 21, 15889

www.rsc.org/materials

COMMUNICATION

A continuous process for Si nanowires with prescribed lengths†

Jungkil Kim,[ab] Hyun Rhu[a] and Woo Lee*[ab]

Received 8th August 2011, Accepted 27th August 2011
DOI: 10.1039/c1jm13831f

A simple top–down approach for the continuous mass preparation of single crystalline silicon nanowires (SiNWs) with controlled lengths was developed. The approach is based on periodic pulsing of anodic bias during gold-assisted chemical etching of a silicon substrate and subsequent ultrasonic treatment of the resulting porosity-patterned SiNWs for selective breakage of nanowires at the porous segments, and allows us to overcome some of the drawbacks in conventional bottom–up methods for SiNW growth.

Introduction

In recent years silicon nanowires (SiNWs) have attracted much attention due to their many unique properties and potential applications as building blocks for advanced electronic devices, biological sensors and optoelectronic devices, as well as for renewable energy devices. As in many applications of nanostructured materials, it is important to synthesize SiNWs with controlled diameter, morphology (*i.e.*, porous *vs.* nonporous), and axial crystal orientation because of close relation between the structure and the physicochemical properties of nanowires (*e.g.*, optical, electrical, and adsorption characteristics of ions or molecules).[1,2] To date, various synthetic methods have been developed for SiNWs with uniform dimensions and crystal orientations. The vapour–liquid–solid (VLS) growth method utilizing catalyst metal nanoparticles is one of the most popular bottom–up approaches for the epitaxial growth of SiNWs with some degree of controllability over diameter and wire density.[3–7] However, tight control over the diameter and spacing of SiNWs is rather difficult to achieve, unless size and location of catalyst metal nanoparticles are lithographically defined on a substrate. In addition, controlled directional growth of SiNWs on silicon substrates of a given orientation is challenging due to the preferred growth directions of SiNWs to ⟨111⟩, ⟨112⟩, and ⟨110⟩ depending on the wire diameter.[4] Moreover, it is difficult to synthesize large quantities of SiNWs on the substrate.[8] Supercritical fluid–liquid–solid (SFLS) and solution–liquid–solid (SLS) growth techniques may allow large-scale synthesis of ultrathin SiNWs.[8–11] Apart from difficulties in controlling the axial crystal orientation of SiNWs due to the preferred nanowire growth along ⟨111⟩ directions, however, these solution-based analogues of the VLS method often require extreme conditions (*i.e.*, $P \approx 100$ bar and $T \approx 450$ °C) either for a supercritical state or for decomposition of organic silicon precursors, and are not suited for the length-controlled synthesis of SiNWs.

In this communication, we report a simple top–down approach for the continuous mass preparation of single crystalline SiNWs with controlled lengths. Our approach is based on periodic pulsing of anodic bias during metal-assisted chemical etching of a silicon substrate using a gold mesh with ordered arrays of nanoholes and subsequent ultrasonic treatment of the resulting porosity-patterned SiNWs for selective breakage of nanowires at the porous segments, and allows to overcome some of the drawbacks in conventional bottom–up growth of SiNWs discussed above (Scheme 1). In our process, the pulse interval defines the length of nanowires, while the size of nanoholes in the gold mesh determines the diameter of SiNWs. Moreover, after nanowire separation by ultrasonic treatment, the remaining gold mesh-loaded silicon substrate can be reused for additional preparation of SiNWs with desired lengths.

Recently, metal-assisted chemical etching of silicon substrates by using thin perforated meshes of noble metals (*e.g.*, Ag, Au, *etc.*) has gained a considerable attention as a promising alternative for controlled fabrication of SiNWs.[12–19] In this process, the silicon that comes in contact with catalyst metal is selectively etched in an aqueous solution containing HF and an oxidant to leave behind ordered arrays of aligned SiNWs, irrespective of the orientation type, doping type and level of the starting silicon substrate. This top–down approach offers several distinct advantages over the conventional bottom–up growths of SiNWs (*i.e.*, VLS, SFLS, and SLS) in terms of control of the axial crystal orientation, morphology, size, and two-dimensional (2D) spatial arrangement of aligned SiNWs, and has been successfully implemented to produce extended arrays of sub-10 nm diameter SiNWs, light-emitting porous SiNWs, nanowires with ribbon-like crosssection, and zigzag or curved SiNWs with controlled turning angles.[2,13,17,18,20]

Results and discussion

Fig. 1a shows a typical electrochemical setup employed in the present study. We utilized a 25 nm thick gold mesh with ordered arrays of nanoholes as a silicon etching catalyst, which could be conveniently

[a]*Korea Research Institute of Standards and Science (KRISS), Yuseong, 305-340 Daejeon, Korea. E-mail: woolee@kriss.re.kr; Tel: +82-42-868-5397*

[b]*Department of Nano Science, University of Science and Technology (UST), Yuseong, 305-333 Daejeon, Korea*

† Electronic supplementary information (ESI) available: (S1) An SEM image of SiNWs formed by applying anodic pulses through direct silicon contact and (S2) a magnified SEM image of silicon wafer after ultrasonic treatment. See DOI: 10.1039/c1jm13831f

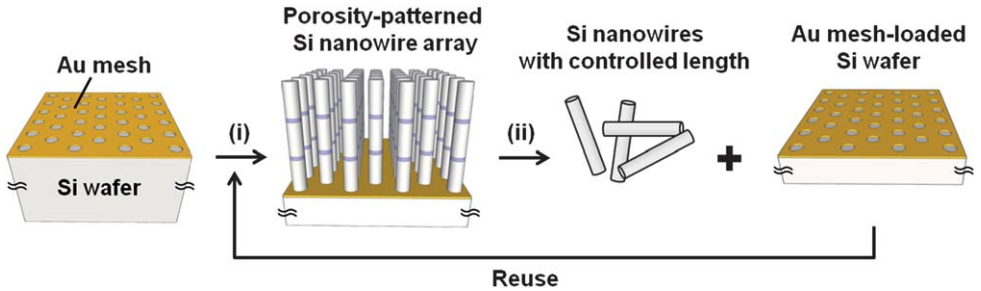

Scheme 1 Schematic diagram of the continued mass fabrication of SiNWs with prescribed lengths by (i) periodic pulsing of anodic bias during metal-assisted chemical etching of a silicon wafer and subsequent (ii) ultrasonic treatment of the resulting porosity-patterned SiNWs. The remaining gold mesh-loaded silicon wafer can be used again for the preparation of SiNWs with desired lengths.

replicated from porous anodic aluminium oxide (AAO) (see Experimental section).[17,18] Chemical etching of the gold mesh-loaded Si(100) wafer (B-doped, resistivity = 1–10 Ω cm) was conducted in an etchant solution comprised of 13.333 M HF and 5.814 M H_2O_2 (ε = [HF]/[H_2O_2] = 2.293) at room temperature, the condition under which silicon was etched at the rate of *ca.* 20 μm min^{-1} to yield vertically aligned nonporous [100] SiNWs. During chemical etching, anodic potential pulses (pulse amplitude = U_{ano}, pulse width = τ_{ano}, and pulse interval = τ_{int}) were applied between the gold mesh and a platinum counter electrode (Fig. 1a and b); the gold mesh was electrically connected to the positive terminal of a computer controlled source/measure unit through a platinum needle that was attached to a micromanipulator, while the platinum counter electrode immersed in the etchant was connected to the negative terminal of a source meter. Fig. 1c shows a representative current (*j*)–time (*t*) transient during chemical etching under anodic potential pulses (U_{ano} = 5 V, τ_{ano} = 0.2 s, and τ_{int} = 3 s). Potential pulsing results in the sharp increase of current density (*j*). Scanning electron microscopy (SEM) image of the resulting sample indicated that SiNWs are aligned vertically and exhibit alternate changes in image contrast along their axes in compliance with the applied potential pulses, in which dark and bright image contrast corresponds to the porous and

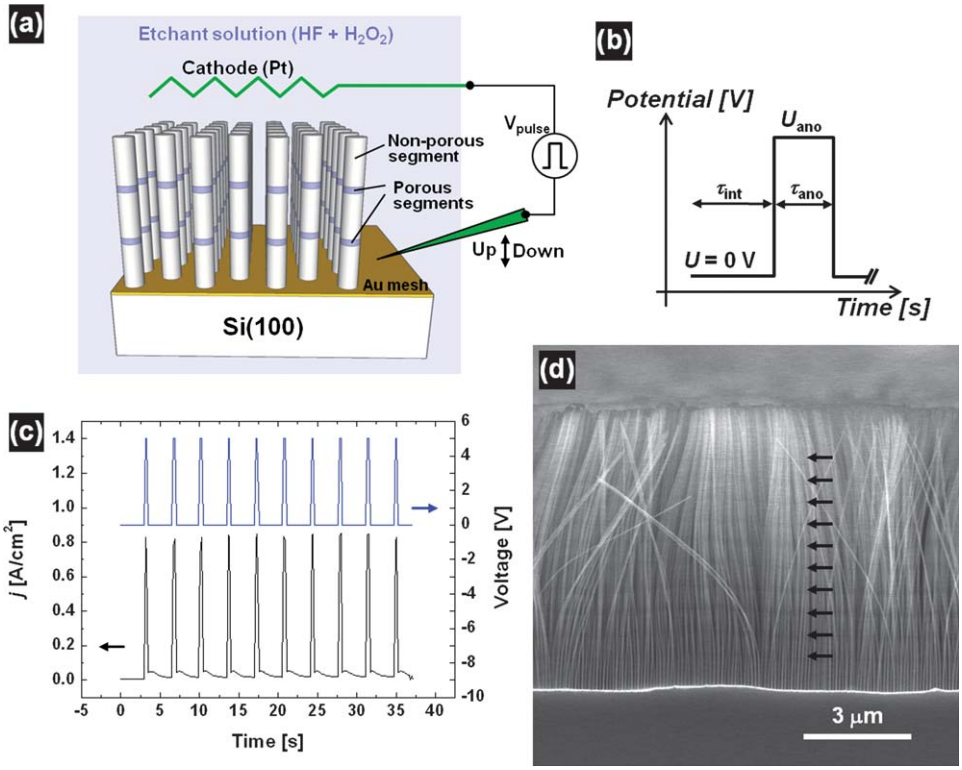

Fig. 1 (a) A schematic showing an electrochemical setup employed for periodic pulsing of anodic potential during metal-assisted chemical etching of silicon; a needle, attached to a micromanipulator and connected to an external power supply is brought into contact with the gold mesh. An external anodic bias is applied between the needle and the Pt-counter electrode immersed in the etchant solution. (b) Pulse scheme used for the present experiment, where U_{ano} and τ_{ano} denote the amplitude and width of anodic potential pulses, respectively, and t_{int} denotes the pulse interval. (c and d) A typical current–time (*j*–*t*) transient during chemical etching of silicon with U_{ano} = 5 V, τ_{ano} = 0.2 s, and τ_{int} = 3 s, and a representative SEM micrograph of the resulting porosity-patterned [100] SiNWs, respectively.

nonporous nanowire segments, respectively (Fig. 1d). The formation of porous nanowire segments by anodic potential pulses could be evidenced by transmission electron microscopy (TEM) investigation (*vide infra*). It should be noted that an applied potential pulse selectively porosifies the area of SiNWs contacting with the gold mesh, without affecting other areas of already formed SiNWs.

Recently, Huang *et al.* have shown that silicon contacting with metal nanoparticles (NPs) can be electrochemically etched under galvanostatic conditions, in which anodic current was supplied from an external current source through a direct contact with Si(111) substrate.[21] They suggested that holes (h^+) injected from the silicon contact diffuse preferentially to the metal nanoparticle/silicon interface (rather than to the solution/silicon interface), because the valence band maximum at the metal nanoparticle/silicon interface is energetically located below compared to that of the electrolyte/silicon interface. In consideration of this report, we applied anodic potential pulses between the silicon substrate (rather than the gold mesh) and the platinum counter electrode and investigated the morphology of the resulting SiNWs as a function of pulse amplitude (U_{ano}). Under anodic bias with low pulse amplitude ($U_{ano} < 1$ V), chemical etching of Si(100) yielded non-porous SiNWs. The etching behavior appeared to be in good agreement with that of Huang *et al.*[21] However, anodic potential pulses with higher pulse amplitude ($U_{ano} > 2$ V) gave rise to severe porosification of the entire surface of SiNWs (especially the top parts of SiNWs) without forming any porosity patterns along the wire axes (see ESI†, S1). The present experimental result indicates that for selective porosification of SiNWs at desired axial locations, externally supplied holes (h^+) should be injected into silicon through the metal contact and not through the silicon. It is practically impossible for one to achieve electrical contact between individual metal nanoparticles and an external power supply. Hence, utilization of an electrically continuous two-dimensional (2D) metal mesh, rather than metal nanoparticles, is important for the preparation of SiNWs with tailor-made porosity patterns by external anodic potential pulses.

Two different electrochemical events are considered to occur in the present etching process. Under the etching condition without anodic bias ($U = 0$ V), the gold mesh acts as an etching catalyst for the reduction of H_2O_2 by utilizing electrons extracted from the underlying silicon through the gold/silicon interface (*i.e.*, injection of positive holes (h^+) into valance band of silicon). In other words, the gold mesh acts as a short-circuited galvanic cell, in which cathodic reaction occurs at the solution/gold mesh interface (eqn (1)), while anodic dissolution of silicon by HF takes place at the gold/silicon interface (eqn (2)).

$$\text{Cathodic rxn.: } H_2O_2 + 2H^+ + 2e^- \rightarrow 2H_2O \quad (1)$$

$$\text{Anodic rxn.: } Si + h^+_{VB} + 6F^- \rightarrow SiF_6^{2-} + 3e^-_{CB} \quad (2)$$

$$\text{Overall rxn.: } Si + 2H_2O_2 + 4H^+ + 6F^- \rightarrow SiF_6^{2-} + 4H_2O \quad (3)$$

Under external anodic potential bias ($U > 0$ V), on the other hand, the 2D gold mesh contacting with silicon does not act as a catalyst, but as an anode. Decomposition of H_2O_2 (eqn (1)) at the solution/gold mesh interface could effectively be suppressed by anodic bias. Instead, the cathodic reaction occurs at the surface of the Pt counter electrode taking electrons from an external power supply. The silicon directly contacting with the gold mesh anode can be oxidized *via* injection of externally supplied positive holes (h^+), and subsequently removed by HF resulting in SiNWs (eqn (2)).

The formation of porous nanowire segments upon applying anodic potential pulses could be explained in terms of the potential-driven localized injection of the extra amount of positive holes (h^+) into silicon through the gold–silicon interface. As discussed above, etching of silicon is a net result of the interplay between the oxidation of silicon *via* the injection of positive holes (h^+) and the removal of oxidized silicon atoms by HF. If the injection of positive holes (h^+) occurs dominantly over the removal of oxidized silicon by HF, there will be an extra amount of generated holes (h^+) that are not consumed by oxidative dissolution of silicon.[15,17] In this case, excess positive holes (h^+) may readily diffuse from the metal/silicon interface to the lattice defects and dopant sites (pore nucleation sites) on the surface of the already formed SiNWs, resulting in nanowire porosification.[18,22–24] In the case of metal-catalyzed etching (*i.e.*, etching without external anodic bias, $U = 0$ V), injection of holes (h^+) is driven by catalytic decomposition of H_2O_2 at the solution/metal interface (eqn (1)).[17] Correspondingly, the etchant composition (*i.e.*, $\varepsilon = [HF]/[H_2O_2]$) plays an important role in determining the morphology (*i.e.*, porous *vs.* nonporous) of the resulting SiNWs. Our recent study on gold-assisted chemical etching of Si(100) wafers indicated that nonporous [100] SiNWs can be obtained at $\varepsilon > 1.2$, while porous [100] SiNWs can be obtained at $\varepsilon < 1.2$ (*i.e.*, etchant solutions with high relative H_2O_2 concentration).[18] In the case of electrochemical etching (*i.e.*, $U > 0$ V), on the other hand, carrier (h^+) injection is driven by the external anodic bias and not by the catalytic decomposition of H_2O_2. Accordingly, the amount of holes (h^+) injected into valence band of silicon would be proportional to the anodic bias (U). In order to verify this argument, anodic potential pulses with different amplitudes ($U_{ano} = 3, 4, 5$ V; $\tau_{ano} = \tau_{int} = 5$ s) were sequentially applied during chemical etching of silicon. Fig. 2 displays electron micrographs of the resulting nanowire sample. It is clear from the SEM micrograph in panel a that the image contrast of porous segments of SiNWs increases with the pulse amplitude (U_{ano}). According to our TEM investigation, the porous segments of SiNWs are characterized by numerous nanoscale voids and interconnected network of nanometre-sized silicon crystallites as shown in Fig. 2e. TEM investigation of SiNWs indicated further that the thickness of porous region along the diameter direction is positively correlated with the pulse amplitude (Fig. 2b–d), supporting our potential-driven hole (h^+) injection mechanism. The present experimental results reveal that one may achieve continuous engineering of the nanowire porosity by simply varying the amplitude (U_{ano}) of anodic pulses during chemical etching.

In our process, pulse duration (τ_{ano}) and pulse interval (τ_{int}) determine the lengths of porous wire segments and nonporous ones, respectively. Correspondingly, SiNWs with tailor-made porosity patterns along their axes can conveniently be prepared by employing potential pulses comprised of two or more different pulse profiles, avoiding the previous tedious periodic exchanges of the etchant solutions to introduce porous wire segments.[16,19] Fig. 3a and b display representative SEM images of [100] SiNWs prepared by applying anodic pulses ($U_{ano} = 5$ V; $\tau_{ano} = 0.2$ s for panel a and $\tau_{ano} = 0.5$ s for panel b) with different pulse intervals (τ_{int}) during chemical etchings of Si(100) wafers; $\tau_{int} = 3$ s for panel a and $\tau_{int} = 8$ s for panel b. Each cross-sectional SEM micrograph shows clearly a series of horizontal lines with a periodic spacing, as indicated by white arrows. These lines with a dark image contrast correspond to the porous nanowire

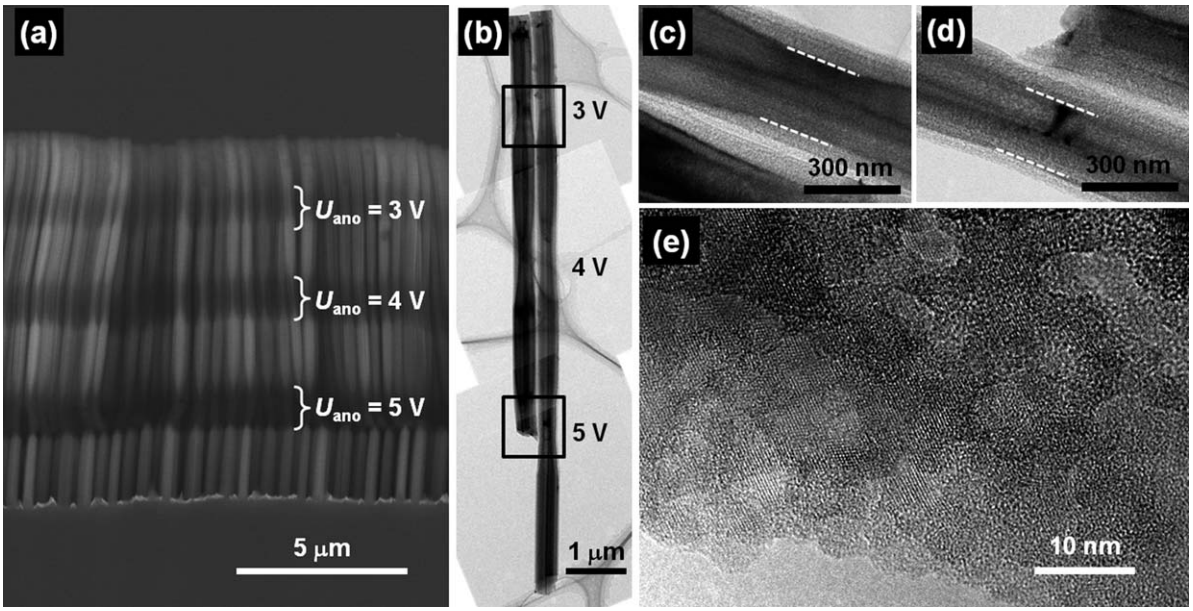

Fig. 2 (a) SEM image of [100] SiNWs prepared by pulsing of anodic bias during metal-assisted chemical etching of Si(100) wafer, showing the effect of pulse amplitude (U_{ano}). (b) TEM micrograph of SiNWs taken from the sample shown in panel a. (c and d) Magnified TEM images of the porous segments formed at $U_{ano} = 3$ V and $U_{ano} = 5$ V, respectively. (e) High-resolution TEM image, showing the morphology of porous segment.

segments formed by anodic potential pulses. On the other hand, the spacing between them corresponds to the length of nonporous wire segments, which is determined by the pulse interval (τ_{int}). The length of porous segment could be as short as 50 nm. It was observed that as-prepared SiNWs are easily broken at the porous segments as marked by a white rectangle in Fig. 3b (see also Fig. 3e). By taking advantage of the weak mechanical nature of the porous wire segments, we were able to obtain nonporous SiNWs with controlled lengths from the as-etched samples by ultrasonic treatment. Fig. 3c and d presents SEM micrographs of [100] SiNWs separated from the samples shown in panels a and b, respectively, demonstrating convenient and reliable control over the length of SiNWs by varying the pulse interval (τ_{int}). It is worth mentioning here that the gold mesh was not separated from the silicon surface maintaining its original

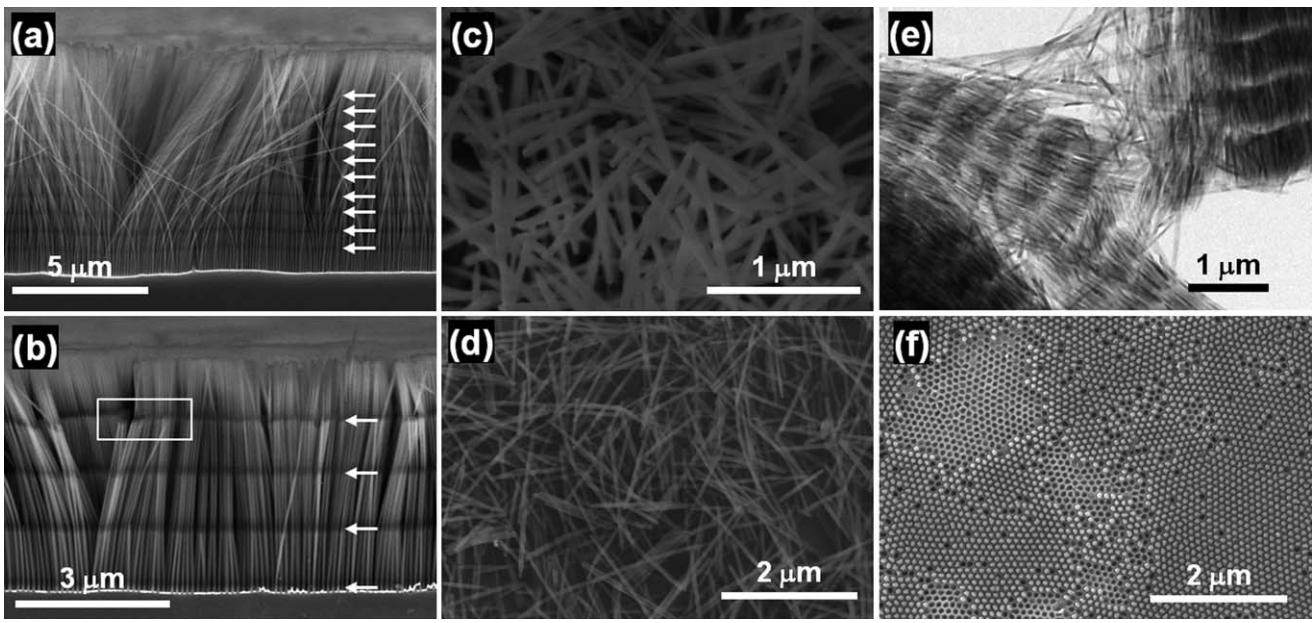

Fig. 3 (a and b) SEM micrographs of [100] SiNWs prepared by pulsing of anodic bias during metal-assisted chemical etching of Si(100) wafer, showing the effect of pulse interval (t_{int}); (a) $\tau_{int} = 3$ s and (b) $\tau_{int} = 8$ s. Other pulse parameters were fixed at $U_{ano} = 5$ V and $\tau_{ano} = 0.2$ s for a and $\tau_{ano} = 0.5$ s for b. For the samples shown in panels a and b, chemical etchings of silicon were terminated with and without anodic potential pulse, respectively. (c and d) SEM micrographs of [100] SiNWs separated from the samples shown in panels a and b, respectively. (e) A typical TEM image of bundles of porosity-patterned SiNWs (before ultrasonic treatment). (f) SEM image of silicon wafer after ultrasonic treatment of the sample shown in (b).

structural details even after the as-etched samples were exposed to an ultrasonic environment to release individual SiNWs (Fig. 3f, see also ESI† S2 for a magnified SEM image). This can be attributed to a conformal contact established between the gold mesh and the underlying silicon surface by chemical etching reaction. Therefore, after nanowire separation by ultrasonic treatment the resulting gold mesh-loaded silicon wafer can be used further for preparing SiNWs with desired lengths, which is one of the attracting features of our nanofabrication process.

Conclusion

In summary, we present a continuous method for the mass production of single crystalline silicon nanowires (SiNWs) with controlled lengths. The approach is based on the periodic pulsing of anodic bias during chemical etching of silicon wafers with catalyst gold mesh in order to yield arrays of multi-segmented SiNWs, in which porous wire segments are regularly sandwiched in-between two nonporous wire segments. It turned out that anodic potential pulses porosify selectively the area of SiNWs contacting with the gold mesh *via* localized injection of externally supplied positive holes (h^+) into the valence band of silicon, in which pulse amplitude determines the porosity of nanowire. In our process, pulse duration and pulse interval determine the lengths of porous wire segments and nonporous ones, respectively. Nonporous SiNWs with uniform lengths could be obtained in mass quantity by ultrasonic treatment of multi-segmented SiNWs aligned on a silicon wafer by taking advantage of the selective breakage of nanowires at the porous segments. After nanowire separation by ultrasonic treatment, the resulting gold mesh-loaded silicon wafer can be used further for preparing SiNWs with desired lengths. The generic capability of tailoring the length of SiNWs could make the present method attractive for developing nanowire-based functional nanostructures.

Experimental section

Pretreatment of Si wafers

The (100)-oriented p-Si wafers (B-doped, ρ = 1–10 Ω cm) or n-Si wafers (P-doped, ρ = 1–10 Ω cm) were cleaned by using either a RCA solution ($NH_3 \cdot H_2O/H_2O_2/H_2O$, v/v/v = 1/1/5) or a Piranha solution (98% H_2SO_4/30% H_2O_2, v/v = 4/1) and then thoroughly rinsed by copious amounts of de-ionized (DI) water prior to use.

Preparation of porous anodic aluminium oxide (AAO)

Free-standing self-ordered porous AAO membranes used for the replication of gold meshes were prepared by potentiostatic anodization of aluminium. In brief, a surface-finished aluminium disc (2 cm in diameter, Goodfellow, 99.999%) was anodized either at 40 V in 0.3 M $H_2C_2O_4$ (1 °C) or at 195 V in 1 wt% H_3PO_4 (1 °C) for 24 h. After anodization the aluminium substrate was removed by using an aqueous mixture solution containing 3.4 g $CuCl_2 \cdot 2H_2O$, 50 mL of 38 wt% HCl, and 100 mL of DI water. Subsequently, the barrier oxide layer at the bottom of pores was removed by using 5 wt% H_3PO_4. Average pore size (D_p) and interpore distance (D_{int}) of the resulting AAO membranes were measured to be D_p = 60 nm and D_{int} = 100 nm for AAO formed at 40 V and D_p = 350 nm and D_{int} = 500 nm for AAO formed at 195 V.

Fabrication of gold mesh

Chemical etching of silicon substrates can be performed by using either isolated nanoparticles or mesh-like porous films of noble metals (*e.g.*, Ag, Au, Pd, and *etc.*) as a catalyst. In the present study, we utilized a thin gold mesh with hexagonal arrays of nanoholes. Unlike conventional approaches using randomly distributed catalyst metal nanoparticles, the present approach allows controlled synthesis of uniform SiNWs, of which diameter, density, and spatial arrangement are predefined by the details of pattern of the catalyst metal mesh. Gold meshes employed in the present work could be conveniently replicated from porous anodic aluminium oxide (AAO) membranes according to the method reported recently.[18] In brief, 25 nm thick Au was sputter deposited onto an AAO membrane. The resulting Au-coated AAO membrane was floated on the surface of 1 M NaOH solution to remove the oxide membrane. After that solution neutralization was carried out by replacing the NaOH solution with DI water. 25 nm thick Au mesh (typical diameter = 1.6 cm) remained floating on the surface of aqueous solution and could be conveniently transferred onto substrates of choice without any structural disintegrations. The edges of nanoholes at the bottom side of the gold mesh were contaminated with loosely connected gold nanoparticles. We removed them from the bottom side of the gold mesh by floating the free-standing gold mesh on the surface of a diluted aqua regia solution for 8 s. After solution neutralization with DI water, the resulting gold mesh was transferred onto the polished surface of silicon wafer. Subsequently, the sample was dried in air to remove the residual amount of water from the interface between the metal mesh and the underlying silicon substrate. The resulting sample was briefly dipped into absolute ethanol. Immediately after that chemical etching of silicon was carried out by immersing the gold mesh-loaded silicon wafer at room temperature.

Microscopic characterization

A Hitachi S-4800 field emission scanning electron microscope (FE-SEM) was employed for the morphological characterization of the samples. The samples were mechanically cleaved for the cross-sectional SEM investigations. The morphology of porosity patterned SiNWs was investigated by a transmission electron microscope (TEM, Tecnai F30, FEI, USA) operated at primary beam energy of 300 kV. To prepare specimens for TEM investigation, the surface of an etched Si substrate was scraped by using a razor blade and nanowires in the scrapings were collected and dispersed in absolute ethanol. A drop of the resulting suspension solution was placed on a carbon-coated Cu grid.

Acknowledgements

This work was supported by Future-based Technology Development Program (Nano Fields) through the National Research Foundation of Korea (NRF) funded by the Ministry of Education, Science and Technology (Grant No. 2010-0029332).

Notes and references

1 C. K. Chan, H. Peng, G. Liu, K. McIlwarth, X. F. Zhang, R. A. Huggins and Y. Cui, *Nat. Nanotechnol.*, 2008, **3**, 31–35.
2 Y. Qu, L. Liao, Y. Li, H. Zhang, Y. Huang and X. Duan, *Nano Lett.*, 2009, **9**, 4539–4543.
3 R. S. Wagner and W. C. Ellis, *Appl. Phys. Lett.*, 1964, **4**, 89–90.

4 V. Schmidt, S. Senz and U. Gösele, *Nano Lett.*, 2005, **5**, 931–935.
5 B. Tian, P. Xie, T. J. Kempa, D. C. Bell and C. M. Lieber, *Nat. Nanotechnol.*, 2009, **4**, 824–829.
6 Y. Cui, L. J. Lauhon, M. S. Gudisen, J. Wang and C. M. Lieber, *Appl. Phys. Lett.*, 2001, **78**, 2214–2216.
7 G. Lee, Y. S. Woo, J.-E. Yang, D. Lee, C.-J. Kim and M.-H. Jo, *Angew. Chem., Int. Ed.*, 2009, **48**, 7366–7370.
8 C. K. Chan, R. N. Patel, M. J. O'Connell, B. A. Korgel and Y. Cui, *ACS Nano*, 2010, **4**, 1443–1450.
9 T. Hanrath and B. A. Korgel, *Adv. Mater.*, 2003, **15**, 437–440.
10 A. T. Heitsch, D. D. Fanfair, H.-Y. Tuan and B. A. Korgel, *J. Am. Chem. Soc.*, 2008, **130**, 5436–5437.
11 J. D. Holmes, K. P. Johnston, R. C. Doty and B. A. Korgel, *Science*, 2000, **287**, 1471–1473.
12 Z. Huang, H. Fang and J. Zhu, *Adv. Mater.*, 2007, **19**, 744–748.
13 Z. Huang, X. Zhang, M. Reiche, L. Liu, W. Lee, T. Shimizu, S. Senz and U. Gösele, *Nano Lett.*, 2008, **8**, 3046–3051.
14 S.-W. Chang, V. P. Chuang, S. T. Boles, C. A. Ross and C. V. Thompson, *Adv. Funct. Mater.*, 2009, **19**, 2495–2500.
15 W. Chern, K. Hsu, I. S. Chun, B. P. de Azeredo, N. Ahmed, K.-H. Kim, J.-M. Zhu, N. Fang, P. Ferreira and X. Li, *Nano Lett.*, 2010, **10**, 1582–1588.
16 J. M. Weisse, D. R. Kim, C. H. Lee and X. Zheng, *Nano Lett.*, 2011, **11**, 1300–1305.
17 J. Kim, H. Han, Y. H. K. S.-H. Choi, J.-C. Kim and W. Lee, *ACS Nano*, 2011, **5**, 3222–3229.
18 J. Kim, Y. H. Kim, S.-H. Choi and W. Lee, *ACS Nano*, 2011, **5**, 5242–5248.
19 C. Chiappini, X. Liu, J. R. Fakhoury and M. Ferrari, *Adv. Funct. Mater.*, 2010, **20**, 2231–2239.
20 A. I. Hochbaum, D. Gargas, Y. J. Hwang and P. Yang, *Nano Lett.*, 2009, **9**, 3550–3554.
21 Z. P. Huang, N. Geyer, L. F. Liu, M. Y. Li and P. Zhong, *Nanotechnology*, 2010, **21**, 465301.
22 C. Chartier, S. Bastide and C. Lévy-Clément, *Electrochim. Acta*, 2008, **53**, 5509–5516.
23 A. G. Cullis, L. T. Canham and P. D. Calcott, *J. Appl. Phys.*, 1997, **82**, 909–965.
24 X. Li and P. W. Bohn, *Appl. Phys. Lett.*, 2000, **77**, 2572–2574.

